Chapter 2

Experimental and Theoretical Techniques

Many spectroscopic techniques have been used in this study, which are connected to the availability of synchrotron radiation. For the reader not familiar with these techniques, the fundamentals are given in this chapter. The experimental techniques are introduced in section 2.1, followed by the theoretical techniques in section 2.2. Both sections summarize existing literature in order to give a flavor of these techniques to the reader. In each section, links to literature with more detailed information are provided.

2.1 Soft X-ray Spectroscopic Techniques

Four techniques are discussed in this section. NEXAFS, RIXS, and XPS have been carried out in the soft x-ray regime. A general schematic presentation for the XAS, XPS, and XES (RIXS) process is presented in Fig.2.1, as it has been published by Winter et. al. [15]. On the other hand, EXAFS has been carried out in the hard x-ray regime.

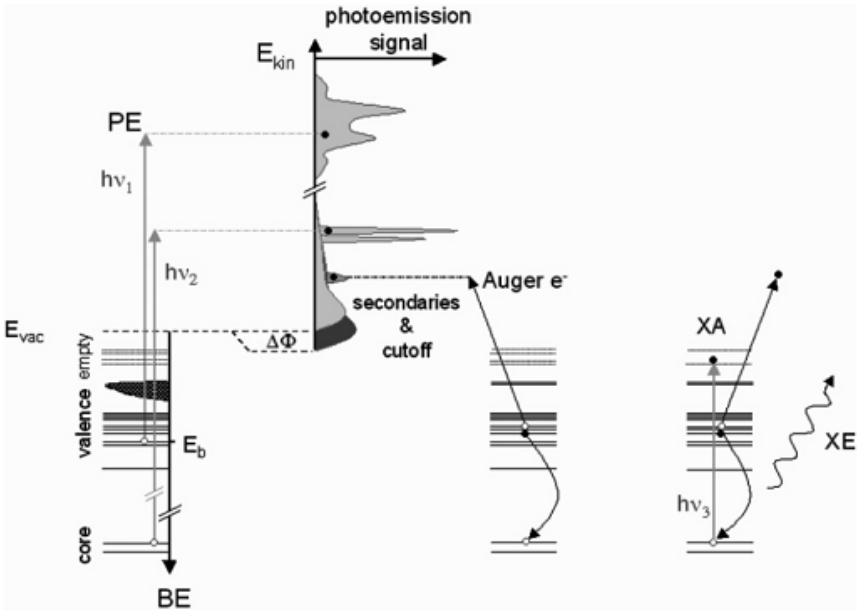

Figure 2.1: (Left) Schematic of the energy levels involved in photoemission. If the photon energy hν exceeds the electron binding energy E_b of a given valence or core level, an electron is ejected from the molecule (ionization), and its kinetic energy E_{kin} is measured. The distribution of E_{kin}(hν) is the photoemission spectrum. In the diagram, electron binding energies, BE, are drawn with respect to the vacuum level, E_{vac}, beyond which the ejected electron is free. The degree to which the measured photoemission spectrum reflects the matrix elements of occupied states varies for different systems and, in addition, depends on the experimental conditions. Adsorbed molecular surface dipoles with a component perpendicular to the surface cause a change of the surface potential $\Delta\Phi$, which results in an energy shift of the low energy cutoff, as indicated in the figure. For the example shown, the surface dipole is assumed to be located in the top surface, the positive charge is up, and the negative charge is down. (Center) Auger electron contribution to the photoemission spectrum that can occur for core-level photoemission. (Right) Illustration of core electron promotion (by $h\nu_3$) into an unoccupied valence state (X-ray absorption; XA). The absorption is probed by (Auger) electron detection or by measurement of emitted x-rays (XE) [15].

2.1.1 NEXAFS

X-ray absorption spectroscopy (XAS) has become an important tool for the characterization of materials as well as for fundamental studies of atoms, molecules, adsorbate, surfaces, liquids and solids [2, 5, 16–18]. The particular assets of XAS spectroscopy are its element specificity and the possibility to obtain detailed information without the presence of any long-range order. Below it will be shown that the x-ray absorption spectrum in some cases is closely related to the empty density of states of a system. As such XAS is able to provide a detailed picture of the local electronic structure of the element studied.

NEXAFS measurements are based on excitation of electrons from a core level to partially filled and empty states in the same system. The peak positions and intensity are directly related to the nature of unoccupied electronic states. Basically, for many of di-atomic molecules like N_2, the NEXAFS spectrum is characterized by a π^* resonance and a set of Rydberg states at energies below the ionization potential (IP), which reflects the energy difference between the core orbital and the vacuum level. Moreover, a σ^* resonance is characterized by a relative broad feature at energies above IP [19]. Probing the excitation of core electrons to unoccupied states, NEXAFS measurements provide direct information about the nature of the empty molecular orbitals. Since the number of empty molecular orbitals and their energy positions are characteristic for different classes of chemical species, NEXAFS spectra can be used as 'fingerprints' for identifying molecular species. As we will show in many of our investigations, NEXAFS features provides a clear finger print for direct ion interaction in solution. Furthermore, because NEXAFS measurements involve dipole transitions from well-defined initial and final states, the application of the dipole selection rule often provides information about the local symmetry of the molecules [18]. This picture is valid in the NEXAFS measurements of inorganic solids such as transition metal compounds, gas, as well as solution.

X-ray Absorption Cross Section

The probability of exciting an electron, from an initial state φ_i to a final state φ_f, by x-ray photons is typically described in terms of the x-ray absorption cross section, σ, which is defined as the number of electrons excited per unit time divided by the number of incident photons per unit time per unit area [18, 19] (It has the dimension of $(length)^2$). Basically, by applying Fermi Golden Rule and by using the dipole approximation [20], σ can be written as

$$\sigma = \frac{4\pi^2 h^2}{m^2}\frac{e^2}{hc}\frac{1}{h\omega}\zeta(E)\left|\langle\varphi_f\left|\hat{e}.\vec{r}\right|\varphi_i\rangle\right|^2\delta(h\omega + E_i - E_f) \tag{2.1}$$

where hω is the incident photon energy, e and m are the charge and mass of electrons respectively, ζ(E) the state density of the final state, $|\langle\varphi_f\left|\hat{e}.\vec{r}\right|\varphi_i\rangle|$ the dipole matrix element, and $\delta(h\omega + E_i - E_f)$ the delta function for the conservation of energy. Eq. 2.1 has been discussed in detail in several reviews [18,19].

An important term in this equation is the dipole matrix term, $|\langle\varphi_f\left|\hat{e}.\vec{r}\right|\varphi_i\rangle|$, reveals the importance of an effective interaction between the electric field, and the unit vector in the direction of the incident x-ray photons. The dipole matrix term is the theoretical basis for the polarization-dependence of NEXAFS measurements. In addition, the nature of the dipole transition also implies that the NEXAFS excitation should obey the dipole selection rule, which states that the change in angular momentum quantum number should be $\Delta l = \pm 1$ between the initial and final states.

Another important term in this equation which is $\zeta(E)$. This term is proportional to the density of final states, thus providing the correlation between a NEXAFS spectrum and the nature of the unoccupied states. Depending on the system studied, electron correlation effects can significantly alter the spectral shape beyond the density-of-states. Furthermore, the final state life-time will typically broaden the spectra features [21].

Detection of NEXAFS

The absorption of an x-ray photon, at a photon energy hν, gives rise to an electronic excitation from the core level to an unoccupied state. As shown in Fig. 2.2, a core hole is created as a result of the excitation. The energy gained by annihilation of the core vacancy can be released by either the radiation of fluorescence photons or by the emission of Auger electrons. The rates of these two de-excitation processes are often respectively termed fluorescence yield (ω_f) and Auger yield (ω_a), and they satisfy the sum rule, $\omega_f + \omega_a = 1$ [22]. The relative ratios of the two decaying channels depend strongly on the atomic number of the element of interest. Nevertheless, some theoretical study compared to the experimental data shows that in some cases the fluorescence yield detection does not exactly measure the magnitude of the x-ray absorption cross section [23]. Experimentally, NEXAFS spectra can be recorded by measuring either the electron yield or fluorescence yield as a function of incident

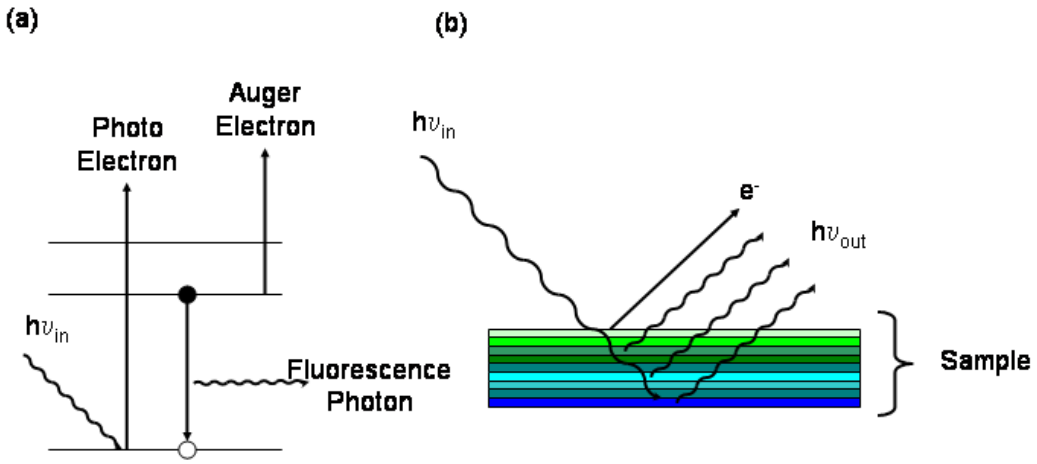

Figure 2.2: (a) Schematics of creation and annihilation of a core hole as result of x-ray interaction with the materials, (b) NEXAFS measurements are carried out by following the de-excitation process, which generates either an Auger electron or a fluorescence photon. As the figure show that the electron yield is surface sensitive and the fluorescence yield is bulk sensitive. (This figure is re-build based on the schematics presented in REF. [19].

photon energy. The fluorescence yield measurement is the most common method used in this thesis. The ability to measure fluorescence yield NEXAFS at the relatively low energy range was first demonstrated near the S K-edge [24] in the mid-1980s. This development represented a major breakthrough in NEXAFS because it provided several new research opportunities. As shown in Fig.2.2.b, fluorescence yield NEXAFS represents a photon-in and photon-out technique, which has three main advantages over the electron yield method: (1) It enables the NEXAFS measurements to be carried out at non-UHV (up to Torr range) conditions, allowing us to measure NEXAFS for liquids in Helium atmosphere. (2) It has a much larger information depth than the electron yield method,

providing an opportunity to probe bulk properties. (3) The detection of photon yield is insensitive to sample charging.

Electron yield can also be measured in atmospheric helium environment, and shows in some cases a stronger signal than the fluorescence. The basic idea is to place a positive electrode next to the liquid to be probed to extract photoelectrons. With the correct electric field strengths and gas pressure, an electron amplification cascade in the Helium can be exploited to amplify the signal.

Normalization of NEXAFS Spectra

The spectra which are measured by NEXAFS can not be directly used. Further analysis has to be done before. Details of these analysis have been published before by J. Stohr [24], nevertheless, I will discuss it shortly in this section in order to show how the data are treated. Normally, the spectra affected by the synchrotron radiation intensity, as well as the beamline optics. The intensity of synchrotron radiation decays as a function of time, typically due to the instability of the electron beam in the storage ring. In addition, the energy-dependent reflectivity changes of the x-ray optics in the beam line introduce an effect. Because the intensity of a raw NEXAFS spectrum depends directly on that of the synchrotron source, the time- and energy-dependent variation in the intensity of synchrotron radiation needs to be removed from the NEXAFS data. This is commonly achieved by placing a fine gold grid directly in the optical path; the simultaneous measurement of photoelectron current from the reference gold grid provides the time- and energy-dependent variation in the radiation source (note that the energy dependent of the reference is insignificant at the probed edge of our samples). In most of our investigations we used the photoelectron signal from the last mirror current, as reference signal. The normalization of NEXAFS data is achieved by dividing the raw NEXAFS spectrum by the concurrently measured reference signal. which is more efficient, since in most cases the last mirror is very clean. Furthermore, in NEXAFS investigations of solute molecules, it is a common practice to normalize with the spectrum of the pure solvent without the solute.

Determination of Self Absorption Coefficients

As the florescence yield signal is often directly proportional to the absorption coefficient, and the signal to background ratio is higher than in case of electron yield measurements, we use this technique in most of our applications. Nevertheless, the experimental FY spectra can exhibit distortions due to so called

'self-absorption effects'. This effects are well described by Eisebit et. al [25]. They report an approach to determine the absorption of concentrated bulk samples by angle dependent FY detection. Moreover, they develop a methodology to calculate the self-absorption effects, which is used in our studies to evaluate this effects as shown in section 4.1.

2.1.2 EXAFS

Discussing EXAFS will shift our interest mostly toward the hard x-ray regime. In the hard x-ray range, photon absorption is mainly determined by core-electron excitations. The dominant one-electron nature of these processes is demonstrated by the existence of main absorption edges corresponding to transitions of 1s (K-edge), 2s (L_1-edge), 2p1/2 (L_2 edge), and 2p3/2 (L_3-edge) electrons to unoccupied states. These edges have a characteristic energy which increases regularly with the atomic number Z. For a given element and absorption channel, the final states involved in the transition depend crucially on their final energy $E_f = E_i + \hbar w$. The photoabsorption process creates a photoelectron with a well defined energy $\hbar w$ - $E_o = \hbar^2 k^2/2m$ (where k is the photoelectron wave-vector and m the electron mass) which escapes from the emitting atom probing its local environment. The final state continuum wavefunction of the photoelectron is influenced by the potentials of the atoms surrounding the photoabsorber resulting in a quantum interference effect visible as an oscillation of the absorption cross-section as a function of the photon energy E = $\hbar w$ [26]. A schematic presentation for EXAFRS principle is presented in Fig.2.3.

The first observations of this phenomenon can be dated to around the year 1920 and were made at the Siegbahn laboratory in Lund (Sweden) [27]. The first comprehensive theoretical treatment was made by Kronig [28, 29] who developed theories suitable for molecules and crystalline solids. This supported by the pioneering theoretical work which done by Hartree et al in this field [30]. The application of EXAFS to the liquid state of matter began even early. Mention of the collection of spectra on aqueous solutions or molecular liquids can be found in several historical papers [31, 32]. Today, EXAFS techniques are used for liquid systems as a standard and direct way for giving information about the local geometric structure of the selected atoms.

The EXAFS signal $\chi(k) = (\mu(E) - \mu_o(E))/\mu_{edge}(E)$, defined as the oscillation of the absorption coefficient $\mu(E)$ with respect to the atomic background $\mu_o(E)$, as a function of the photoelectron wavevector $k = \sqrt{2m(E - E_o)/\hbar}$, and

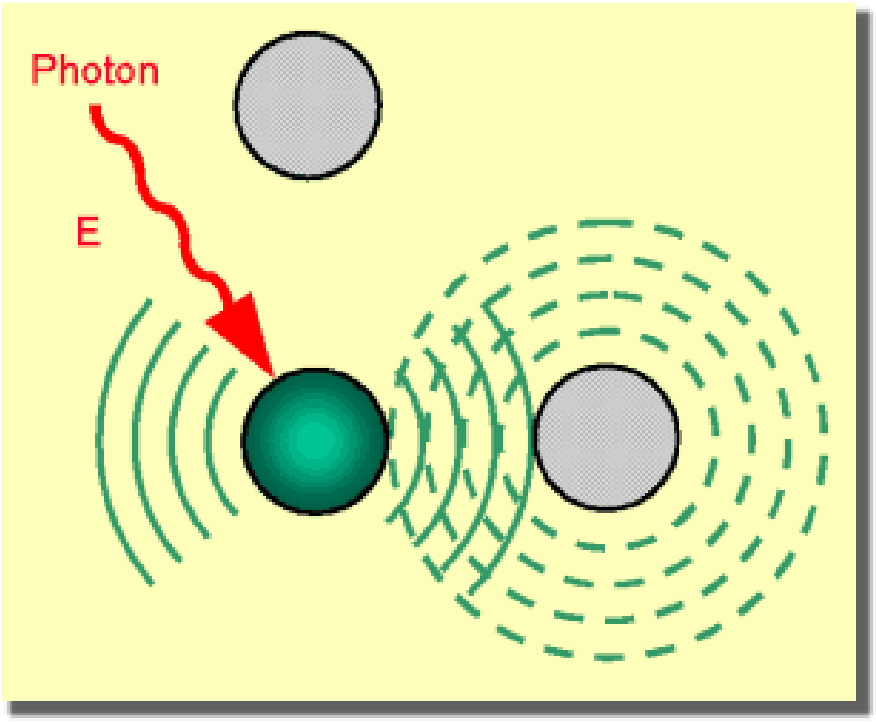

Figure 2.3: The interference of emitted and reflected photo-electron waves by EXAFS technique provides information about the local environment of the selected atom.

normalized to the atomic cross-section of the edge under consideration $\mu_{edge}(E)$. It can be written as the sum of single scattering contributions from each shell j equivalent neighbors with a Gaussian distribution of variance σ_j^2 around the average distance R_j. For a K-edge and after a polarization average one obtains

$$\chi(k) = \sum \frac{N_j}{kR_j^2} e^{-2R_j/\lambda_j(k)} \, |f_j(k,\pi)| \, sin(2kR_j + 2\delta_1'(k) + \phi_j(k)) e^{-2\sigma_j^2 k^2} \qquad (2.2)$$

Where $|f_j(k,\pi)|$ and $\phi_j(k)$ are the back scattering amplitude and phase function of the neighbors j, $\delta_1'(k)$ is the $l = 1$ phase-shift for the photo-absorber atom, and $\lambda_j(k)$ is a phenomenological mean-free-path term accounting for inelastic losses. In spite of the numerous approximations contained in this approach and the inadequacy of a Gaussian shell model for describing atomic distributions in liquids, this expression is still commonly used to interpret spectra of liquid samples. In a general expression the sum over the shells and the so called EXAFS Debye–Waller factor $\exp(-2\sigma_j^2 k^2)$ are substituted by a proper integration over a pair distribution function g(r).

2.1.3 RIXS

Resonant inelastic x-ray scattering (RIXS) is a tool for the study of the electronic structure of matter. It gives unique information about the valence electrons of a system, which is complementary to that of valence band photoemission spectroscopy [33, 34]. The RIXS spectra can often be interpreted in a simple scheme, in which case one gets a map of the selective momentum $\vec{k}$. However, electron correlation has to be taken into account in the interpretation of the spectra. In general the excitation and the decay can not be separated and the entire scattering process is described by the Kramers-Heisenberg formula (the formula described in book by Sakurai [35]). Often, however, a simplified two-step interpretation is suitable where absorption and emission can be seen a separated events. With the use of monochromatic synchrotron radiation as excitation the possibility to study materials can be done in great details. Recently the technique has been increasingly applied in liquid phase samples at Berkeley lab (ALS) [1–3].

The binding energy of a core level is strongly influenced by the chemical environment. Consequently, the position of the absorption threshold is also influenced by the chemical environment. If one atomic species is present in inequivalent positions, the NEXAFS spectrum is a superposition of spectra of the different species in the samples. In general the x-ray emission is also a superposition of many species. By tunning the excitation energy to a certain feature in the absorption features of the atomic species, one can excite a special species to be probed. This is one main advantages of the RIXS technique.

2.1.4 XPS

A comprehensive discussion for the XPS technique is presented in REF. [36]. The photoelectric effect was experimentally discovered by Hertz in 1887 [37]. The theoretical explanation was given by Einstein in 1905 [38], for which he got the Nobel price in physics in 1921. Photoelectron spectroscopy has been developed by the pioneering work of Kai Siegbahn's group in Uppsala in the 1960's. Siegbahn was awarded the Nobel prize in physics in 1981 for this work. His work is the basis for the use of this technique in chemical characterization of materials. This technique has been named electron spectroscopy for chemical analysis (ESCA) [39, 40]. The basic idea is that the binding energy of an electron in a molecular orbital of the molecule will be affected by the nature of its chemical environment (chemical shift).

XPS refers to the ionization of an energy level (energy E_b), which requires absorption of a photon energy with h$\nu > E_b$. The kinetic energy distribution of photoelectrons, E_{kin}(hν), ejected from all possible occupied states is the XPS spectrum, which one measures in experiments using a suitable electron energy analyzer. Energy conservation then yields

$$E_{b,i}(N) + h\nu = E_{b,f}(N-1,k) + E_{kin} \tag{2.3}$$

where $E_{b,i}$(N) denotes the energy of the initial state of the N-electron system. $E_{b,f}$(N - 1,k) is the energy of the final state, i.e., of an ion plus a photoelectron with kinetic energy E_{kin}; k is the initial level from which the electron was removed. This relationship between binding energy, excitation energy, and electron kinetic energy is schematically illustrated in Fig.2.1 (taken from REF. [15]). For relatively low photon energies, the lower binding energy levels (valence states) can be ionized, whereas both valence and core states can be ionized when higher photon energies are used. In the case of inner-shell excitation, Auger electrons appear in the photoelectron spectrum. They result from nonradiative decay of the initial core hole, involving the filling of the core hole by an outershell electron, with the released energy being imparted to another valence electron, which then escapes into vacuum with a kinetic energy characteristic of the system.

2.2 Theoretical Modeling

As discussed before NEXAFS, RIXS, as well as XPS are powerful methods to study the local electronic structure around an absorbing site of various types of matter. Electronic structure calculations for specific geometrical models allow to calculate spectra which can be compared to the experimental data. Upon comparing the simulated spectra with the experimental ones, one can get detailed electronic structure information, as well as some geometrical structure information. EXAFS is gives direct information about the local geometrical structure, and the FEFF modeling package allows to extract quantitative parameters upon comparing the simulated spectra with the experimental one.

2.2.1 Gaussian

Gaussian is capable of predicting the properties of molecules, as well as the path way of chemical reactions. In general, the program is able to do many different calculations, more specifically for our application:

- Molecular energies and structures
- Energies and structures of transition states
- Bond and reaction energies
- Molecular orbitals
- Atomic charges and electrostatic potentials
- Vibrational frequencies
- Thermochemical properties

Recently, simulating solvation field is possible in Gaussian 03. This option will be of important for the work presented in this thesis, since most of the research in this thesis carried out in the liquid phase. In the following sections, the focus will be on the Gaussian tools which have been used in this thesis.

Single point energy calculation

A single point energy calculation is a prediction of the energy and related properties for a molecule with a specified geometric structure. Energy level means the sum of the electronic energy, and the nuclear repulsion and kinetic

energy of the molecule at the specified nuclear configuration. In general this quantity is referred to as the total energy. However, more complete and accurate energy predictions require a thermal or zero-point energy correction, as will be shortly discussed later. The validity of the results of these calculations depends on having reasonable structures for the molecules as input.

Single point energy calculations are performed for many purposes, including the following:

- Obtain basic information about molecular orbitals
- Consistency check on a molecular geometry to be used as the starting point for an optimization
- Compute very accurate values for the energy and other properties for a geometry optimized at a lower level of theory
- Sometimes, it is the only computationally affordable calculation for a system of interest

In all cases, it can be performed at any level of theory and with small or large basis sets. In this studies, it is mainly performed either with Hartree-Fock method, or with density functional theory (DFT) technique. Details about these electronic structure calculation methods have been discussed in detail in Ref. [41].

Geometry optimization

The way the energy of a molecular system varies with small changes in its structure is specified by its potential energy surface. The potential energy surface is a mathematical relationship linking molecular structure and the resultant energy. Geometry optimizations usually attempt to locate minima on the potential energy surface, thereby predicting equilibrium structures of molecular systems. Optimizations can also locate transition structures.

A geometry optimization begins at the molecular structure specified as its input, and steps along the potential energy surface. It computes the energy and the gradient at that point, and then determines how far and in which direction to make the next step. The gradient indicates the direction along the surface in which the energy decreases most rapidly from the current point as well as the steepness of that slope.

Frequency calculations

This calculation is not directly connected to our experimental techniques, but it serves a number of different purposes:

- As a direct output is the IR and Raman spectra of molecules (frequencies and intensities)
- Compute force constants for a geometry optimization
- Identify the nature of stationary points on the potential energy surface
- Compute zero-point vibration and thermal energy corrections to total energies as well as other thermodynamic quantities of interest such as the enthalpy and the entropy of the system

Raw frequency as well as zero-point energy (ZPE) values computed at the Hartree-Fock level contain known systematic errors due to the neglect of electron correlation, resulting in overestimates of about 10%-12%. Therefore, it is common to scale frequencies predicted at the Haretree-Fock level by an empirical factor of 0.8929. The use of this factor has been demonstrated to produce very good agreement with experiment for a wide range of systems [42].

Frequencies and ZPE computed with methods other than Hartree-Fock are also scaled to similarly eliminate known systematic errors in calculated frequencies. The following table lists the recommended scale factors for frequencies and for ZPE Tab.2.1 [43].

	Scale Factor	
Method	Frequency	ZPE/Thermal
HF/3-21G	0.9085	0.9409
HF/6-31G(d)	0.8929	0.9135
MP2(Full)/6-31G(d)	0.9427	0.9646
MP2(FC)/6-31G(d)	0.9434	0.9676
SVWN/6-31G(d)	0.9833	1.0079
BLYP/6-31G(d)	0.9940	1.0119
B3LYP/6-31G(d)	0.9613	0.9804

Table 2.1: Scale factors for frequencies and ZPE.

Modeling systems in solution

One of the useful tools in Gaussian03 is the ability to model systems in solution. Modeling solutions in Gaussian is done via Self-Consistent Reaction Field (SCRF) methods. The simplest SCRF model is the Onsager reaction field model. In this method, the solute occupies a fixed spherical cavity of radius a_o within the solvent field. A dipole in the molecule will induce a dipole in the medium. In turn, the electric dipole field of the medium interact with the molecular dipole leading to final net stabilization.

Tomasi's Polarized Continuum Model (PCM) is one of the models which has used in many of our investigations. It defines the cavity as a union of a series of interlocking spheres around the atoms. The effect of polarization of the solvent continuum is represented numerically.

The two isodensity surface-based SCRF models also use a numerical representation of the solvent. The Isodensity PCM (IPCM) model defines the cavity as an isodensity surface of the molecule. It basically uses an SCRF cycle to perform and converge the isodensity cavity. The cycle repeat until the cavity shape no longer changes upon completion of the SCRF. The result is a very natural, intuitive shape for the cavity since it corresponds to the reactive shape of the molecule to as great a degree as is possible.

The Self-consistent Isodensity Polarized Continuum Model (SCI-PCM) is designed to combine the isosurface effect as well as the electron density effect. It includes the effect on solvation in the solution of the SCRF conversion. this procedure solves for the electron density which minimizes the energy, including the solvation energy, which itself depends on the cavity, as a consequence, it depends also on the electron density. In other words, the effects of solvation are folded into the iterative SCRF computation rather than comprising an extra step afterward.

Theoretical details behind each model are found in the literature. For the Onsager Reaction Field Model, REF. [44], REF. [45], for SCI-PCM Model, REF. [46], in general for SCRF REFs. [47].

2.2.2 StoBe

This program package help us to calculate NEXAFS spectra for Na, Mg, K, Ca, Al, P, S, N, and oxygen. The package has been explained in detail in many articles [48–52]. In this section, I give a brief summery about the program summarized from these previous articles, and show one example calculation at the end. The StoBe program considers the orbital-based Kohn-Sham (KS) equations

$$H_{KS}\phi_i = \epsilon_i\phi_i \tag{2.4}$$

where H_{KS} is the local operator with the exchange-correlation potential $V_{xc}[\rho(\bar{r})]$, and ϕ_i is the wave function

$$H_{KS} = -\frac{1}{2}\nabla^2 - \sum_N \frac{Z_N}{|r_N - r|} + \int \frac{\rho(r')}{|r - r'|}dr' + V_{xc}[\rho(\bar{r})] \tag{2.5}$$

where the sum runs over 'N' nuclei, with r_N being the nuclear nuclei coordinate, and r the electron coordinate,

and

$$\rho(\bar{r}) = \sum_i^{occ}\sum_s^{spin} n_i \left|\phi(\bar{r}, s)\right|^2 \tag{2.6}$$

and utilize the implementation of this equation in the StoBe. The transition state with a half-electron in the core orbital is participating in the x-ray absorption as well as emission. The transition potential (TP) method is useful in cases where Koopman's theorem fails, as for core ionization, and has been implemented in several MSX_α, Hartree-Fock, and DFT schemes [53–55]. The orbitals for the molecule are determined using a good quality molecular basis set with a half-occupied core-orbital at the ionization site. The orbitals for the excited electrons are then obtained by diagonalizing the Kohn–Sham matrix built from the former density matrix in a basis set extended by a large set of diffuse basis functions (150–400 functions) centered on the excited atom. The obtained orbital energies and computed transition moments provide a representation of the excitation energies and associated intensities in the theoretical spectrum. The TP calculation gives most of the relaxation effect upon core- ionization and provides a single set of orthogonal orbitals for the spectrum calculation. In order to determine the absolute energy position of the spectrum, Delta Kohn–Sham (ΔKS) calculations, i.e., allowing full relaxation of the fully ionized core hole

state, were performed to compute the relaxed ionization energy (IP). In the ΔKS-calculations the non core-excited atoms were described by effective core potentials (ECP). This simplifies the definition of the core hole state, since the use of an ECP description eliminates the 1s level of the atom to which it is applied. This is very helpful in core–hole calculations for an atom, which is not the only one of its kind in the studied molecule. The ECPs introduce insignificant effects on the computed spectrum [52].

Nevertheless, this TP neglects the relaxation effects on the molecular ion core on adding the excited electron. On the other hand, this effect is largest for the valencelike π^* excitations and, for that, these states are computed with fully relaxed ΔKS calculations. The core-excited states were variationally determined with maintained orthogonality between the excited states, and done as follows: The first excited state is obtained by fixing the occupation of the core spin orbital to zero and placing the excited electron in the first π^* orbital. A full relaxation with this constraint leads to a state that is almost orthogonal to the ground state due to the $1s^{-1}$ configuration. The next state is then obtained by removing the variationally determined π^* orbital from the variational space and occupying the next level. This procedure gives a variational lower bound to the energy and guarantees orthogonality between the excited states since all remaining orbitals now have to be orthogonal to the eliminated π^* level-(s). The corresponding peaks in the energy-shifted TP spectrum have been shifted to include the additional relaxation effects obtained from the specific ΔKS excited state calculations. In Fig.2.4, I present StoBe simulation for sodium K-edge (NaCl salt solid) compare to the experiment.

The spectrum is generated by a Gaussian convolution of the discrete spectrum with varying broadenings. More specifically, for many of our investigation, for the region below the ionization threshold the broadening [full width at half maximum (FWHM)] is 0.2 eV, for the next 15 eV the FWHM was linearly increased up to 3.0 eV and at higher energies a constant broadening of approximately 3.0 eV is applied. In most of the calculation, the stability analysis of the convoluted spectra with respect to the augmentation basis is investigated by first extending the augmentation basis to include the excitation basis also on the nearest neighbors. The exponents in the basis are furthermore scaled up and down by 5% relative to the original augmented basis set.

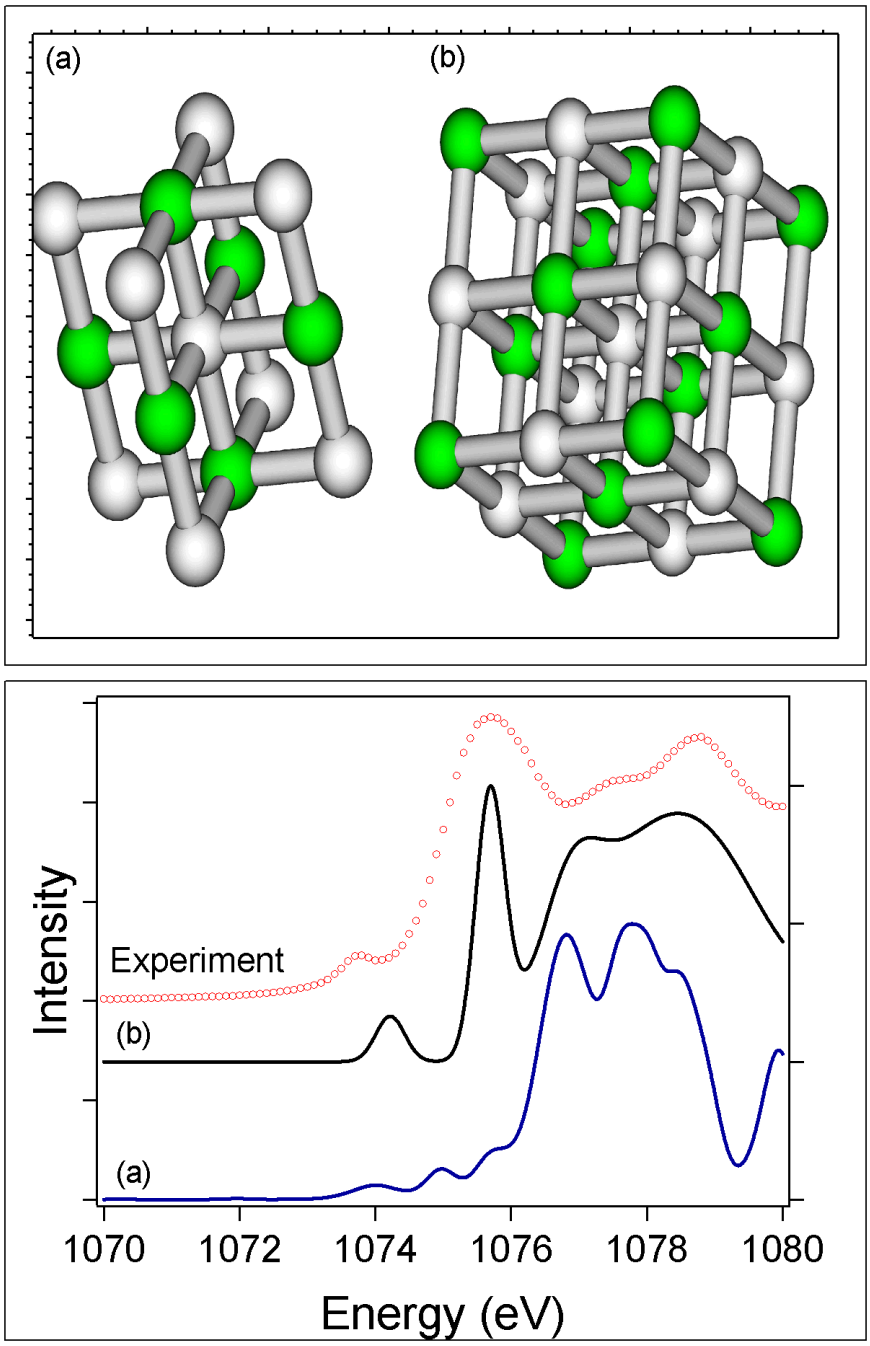

Figure 2.4: In the bottom, Na K-NEXAFS spectra for the crystal form of NaCl measured at U41/PGM (red) are compared to the simulated spectra using StoBe deMon package. The calculation shows the effect of the 2^{nd} neighbor. In the top, we present the two models for the crystal used as an input, where (a) includes the first nearest neighbor atoms, and (b) includes the 1^{st} and the 2^{nd} neighbor atoms. Note that the green sphere is the Cl atom, and the gray is the Na atom.

.

2.2.3 Multiplet Calculations

The single particle description of x-ray absorption works well for all K edges and a range of dedicated computer codes exist to calculate the x-ray absorption cross-section. For this, the StoBe program was sufficient enough to calculate the K edge, as has been discussed in section 2.2.2, and it gives a good description for the K-edge of Na (presented in this thesis), as well as K-edge of Mg, Al, Nitrogen, Carbon, and Oxygen which are not presented in this thesis. Other dedicated codes have been presented in the review of John Rehr as well as the latest developments in the single electron codes using multiple scattering [56, 57]. Cabaret and co-workers describe the new developments in band structure codes and the recently developed PARATEC-based projection method promises to set a new standard for single electron XANES calculations [58]. Applying these one-electron codes (where one-electron applies to a one-electron core excitation, not to the treatment of the valence electrons) to systems such as transition metal oxides or halides one finds excellent agreement for the metal and oxygen K edges, whereas for the other edges, in particular the metal $L_{2,3}$ edges, the agreement is poor. The reason for this discrepancy is not that the transition matrix is calculated wrongly, but that one does not observe the density of states in such x-ray absorption processes. The reason for the deviation from the transition matrix is the strong overlap of the core wave function with the valence wave functions, as well as valence - valence interaction. This overlap of the wave functions is present also in the ground state, but because all core states are filled, it is not effective and one can approximate the core electrons with their charge. In the final state of an x-ray absorption process a partly filled core state, for example, a $2p^5$ configuration is existing. In case of investigating a system with a partly filled 3d-band, for example, Ni^{+2}, the final state will have an incompletely filled 3d-band. For Ni^{+2} this can be approximated as a $3d^9$ configuration. The 2p-hole and the 3d-hole have radial wave functions that overlap significantly. This wave function overlap is an atomic effect that can be very large. It creates final states that are found after the vector coupling of the 2p and 3d wave functions. This implies that the atomic multiplet effects are of the same order of magnitude in atoms and in solids.

In case of s core holes, multiplet effects are effectively reduced to just the exchange interaction between the spin of the s core hole and the spin of the valence electrons. The 1s core states have in all cases a very small exchange interaction, implying that multiplet effects will not be visible significantly. This implies that single electron codes will be effective for all K edges. For multiplet

effects to have a significant effect on the mixing of the L_3 and L_2 edges, the value of the Slater–Condon parameters must be at least of the same order of magnitude as the spin–orbit coupling separating the two edges. If the core spin–orbit coupling is large, there still can be an effect from the Slater–Condon parameters. For more details discussion about the multiplet effects in x-ray spectroscopy, I recommend for the reader the review paper of Frank de Groot [59]. In Fig.2.5 I present the initial and final state effects, 2p spin-orbit coupling, slater-condon parameter and the 3d spin-orbit coupling on the simulated NEXAFS spectra for Ni

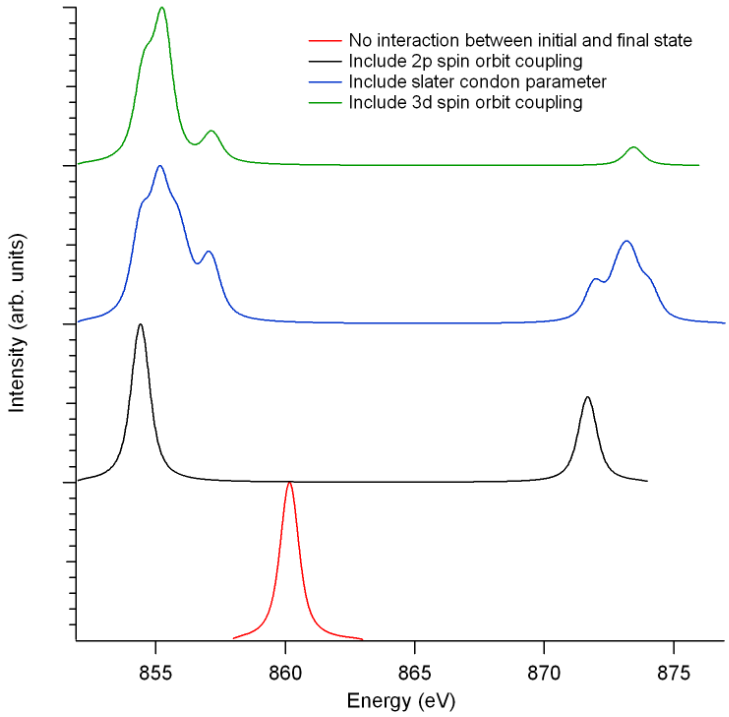

Figure 2.5: NEXAFS L-edge simulation for Ni(Cowan package).

2.2.4 FEFF8

FEFF8 is able to calculate extended x-ray-absorption fine structure (EXAFS), x-ray-absorption near edge structure (XANES), x-ray natural circular dichroism (XNCD), spin-dependent calculations of x-ray magnetic dichroism (XMCD) and spin polarized x-ray absorption (SPXAS and SPEXAFS), nonresonant x-ray emission (XES), electronic structure including local densities of states (LDOS), and the x-ray elastic scattering amplitude. Electron energy loss (EELS) can also be calculated, but it is not an automated feature in this release. In my study, I use the program for calculating modeling EXAFS spectra for the K-edge of transition metals. Nevertheless, before modeling EXAFS spectra, the experimental data should be reduced first, followed by modeling. In this section, a brief introduction for the reduction of the experimental EXAFS data, as well as modeling using FEFF8 is given. The principal investigator of the FEFF project is John J. Rehr [60].

EXAFS Data Reduction

No matter whether μ(E) is measured in transmission or fluorescence (or electron emission), the data reduction and analysis are essentially the same. In this section I will explain briefly the data reduction on one of our measurements for the hydrated powder of $NiCl_2$. The data reduction has been done as follow: first subtract a smooth pre-edge function from μ(E) to get rid of any instrumental background and absorption from other edges, as it is shown in Fig.2.6. The second step is to identify the threshold energy E_0, typically as the energy of the maximum derivative of μ(E). Then normalize the μ(E) edge jump to go from 0 to 1, as it shown in Fig.2.7. The normalized spectra go through two steps, first convert to the k space, as shown in Fig.2.8, then apply the Fourier Transform, as shown in Fig.2.9.

EXAFS Data Modeling

The FEFF program can calculate the scattering amplitude and phaseshifts theoretically. These results of the FEFF calculation are stored in simple files containing the scattering factors and mean-free path for a given coordination shell. The calculations in these files can be used directly in a number of analysis programs. Once the theoretical scattering factors are obtained, one can use them in the EXAFS equation to refine structural parameters from the data. That is, we'll use the calculated functions f(k) and δ(k) (and also λ(k)) in the EXAFS equation to predict and modify the structural parameters R, N, and σ^2 and also allow E_0

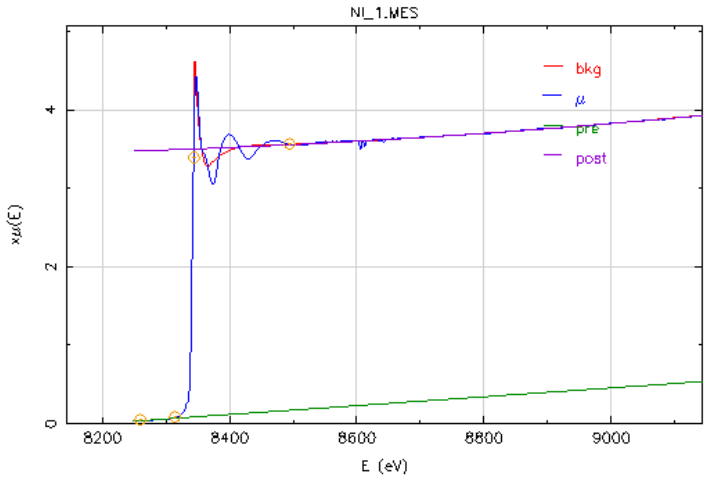

Figure 2.6: Subtraction of the background from EXAFS measurement for $NiCl_2$ hydrated powder using the K-edge of the Ni.

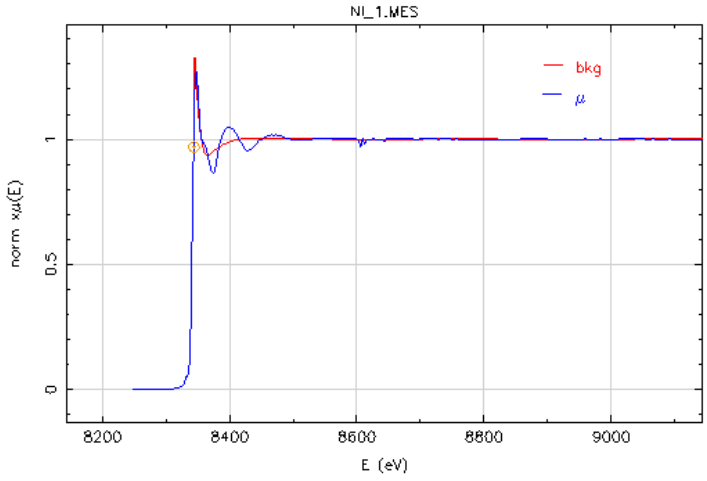

Figure 2.7: Normalized EXAFS spectra for $NiCl_2$ hydrated powder at the K-edge of Ni.

to change until it gets the best-fit to the χ(k) of the data. Alternatively, the fitting can be performed in Fourier space. Structure parameters are extracted from the comparison of the calculated EXAFS spectrum with the experimental data. The results of the fitting calculations for Ni^{2+} in solid and liquid at different concentration will be presented in section 4.4.

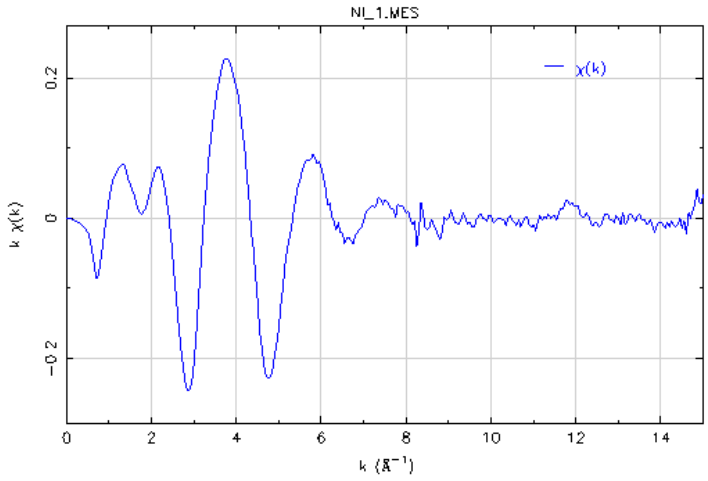

Figure 2.8: EXAFS spectra for $NiCl_2$ hydrated powder at K-edge of Ni converted to the k-space.

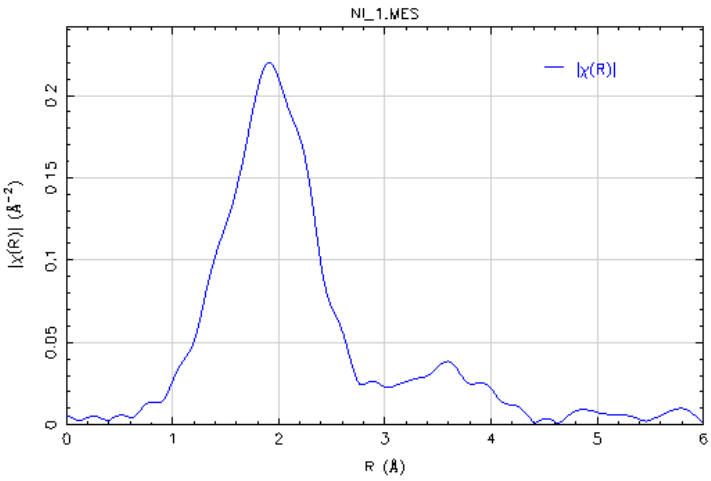

Figure 2.9: The Fourier Transform for the EXAFS spectra for hydrated $NiCl_2$ powder at the K-edge of Ni. From the radial distribution function, the $d(Ni - OH_2) = 1.9\mathring{A}$ (the position of the main peak). More details about this measurements will be presented in section 4.4.2.